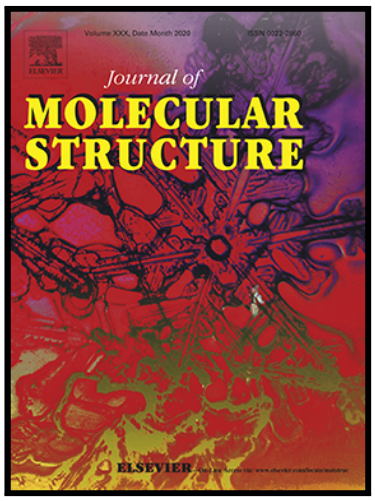


# A ZINC-BASED COORDINATION POLYMER AS ADSORBENT FOR REMOVAL OF TRICHLOROPHENOL FROM AQUEOUS SOLUTION: SYNTHESIS, SORPTION AND DFT STUDIES

Adetola C. Oladipo , Adedibu C. Tella , Hadley S. Clayton , Victoria T. Olayemi , Oghenerobor B. Akpor , Tendai O. Dembaremba , Adeniyi S. Ogunlaja , Guy J. Clarkson , Richard I. Walton

PII: S0022-2860(21)01403-4
DOI: https://doi.org/10.1016/j.molstruc.2021.131274
Reference: MOLSTR 131274

To appear in: *Journal of Molecular Structure*

Received date: 15 December 2020
Revised date: 5 August 2021
Accepted date: 8 August 2021

Please cite this article as: Adetola C. Oladipo , Adedibu C. Tella , Hadley S. Clayton , Victoria T. Olayemi , Oghenerobor B. Akpor , Tendai O. Dembaremba , Adeniyi S. Ogunlaja , Guy J. Clarkson , Richard I. Walton , A ZINC-BASED COORDINATION POLYMER AS ADSORBENT FOR REMOVAL OF TRICHLOROPHENOL FROM AQUEOUS SOLUTION: SYNTHESIS, SORPTION AND DFT STUDIES, *Journal of Molecular Structure* (2021), doi: https://doi.org/10.1016/j.molstruc.2021.131274

Highlight

- A zinc coordination polymer, $[Zn(hba)_2(tmdp)]_n$ (**1**), (where Hhba = 4-hydroxybenzoic acid and tmdp = 4,4'-trimethylenedipyridine) was synthesized in ethanol and water.
- (**1**) was characterized using microscopic, spectroscopic, X-ray diffraction and thermogravimetric techniques.
- (**1**) was found effective for 2,4,6-Trichlorophenol(TCP) adsorption, with an adsorption capacity of 207.8 mg/g.
- DFT Studies were carried out to investigate interaction between 1 and TCP

# A ZINC-BASED COORDINATION POLYMER AS ADSORBENT FOR REMOVAL OF TRICHLOROPHENOL FROM AQUEOUS SOLUTION: SYNTHESIS, SORPTION AND DFT STUDIES

Adetola C. Oladipo[a,b], Adedibu C. Tella[b,c] , Hadley S. Clayton[c] , Victoria T. Olayemi[b,d] Oghenerobor B. Akpor[e], Tendai O. Dembaremba[f], Adeniyi S. Ogunlaja[f], Guy J. Clarkson[g], Richard I. Walton[g]

[a]Department of Physical Sciences, Landmark University, Omu-Aran, Nigeria

[b]Department of Chemistry, P.M.B.1515, University of Ilorin, Ilorin, Kwara State, Nigeria

[c]Department of Chemistry, University of South Africa, Pretoria, South Africa

[d]Department of Chemistry, College of Pure and Applied Sciences, Kwara State University, P.M. B 1530, Malete, Nigeria

[e]Department of Biological Sciences, Afe Babalola University, PMB 5454, Ado-Ekiti, Nigeria

[f]Department of Chemistry, Nelson Mandela University, P.O. Box 77000, Port Elizabeth, 6031, South Africa.

[g]Department of Chemistry, University of Warwick, Coventry, CV4 7AL, UK

**Abstract**

$[Zn(hba)_2(tmdp)]_n$ (**1**), a Zn-coordination polymer (CP), prepared by the reaction of $Zn(NO_3)_2 \cdot 6H_2O$ , 4-hydroxybenzoic acid (Hhba) and 4,4'- trimethylenedipyridine (tmdp) was reported. The compound was characterised, using CHN, single crystal and powder X-ray diffraction analysis, FT-IR, and TGA techniques. It exhibits a square pyramidal geometry, with the zinc (II) atom coordinated to two nitrogen atoms from two tmdp ligand molecules and to three oxygen atoms from two hba molecules. The zinc (II) carboxylate units are bridged through the N-donor spacer ligand, thereby giving rise to a one-dimensional CP. PXRD analysis confirmed the purity of the bulk of (**1**)**.** Compound (**1**) presented an adsorption capacity of 207.8 mg/g for the removal of 2,4,6-trichlorophenol (TCP) from aqueous solution. The adsorption mechanism is governed by π-π stacking and electrostatic interactions, as obtained from DFT studies. The feasibility and exothermic nature of the adsorption process is indicated by the negative binding energy obtained.

**Keywords:** $[Zn(hba)_2(tmdp)]_n$; Coordination polymer; adsorption; DFT studies; trichlorophenol

## l. **Introduction**

In recent years, a class of compounds known as coordination compounds have received a great deal of attention. They are crystalline and their structures are made up of infinite array of metals bridged by organic ligands to form 1D (chains), 2D (sheets) or 3D (frameworks) structures. Their porous counterparts are known as metal organic frameworks (MOFs). They are materials with interesting properties and potential applications like gas and liquid phase adsorption, sensing, photocatalysis, luminescence, drug delivery, antibacterial applications etc.[1–7]. Therefore, there is an increased interest on the development of novel CPs suitable for the intended application. More interestingly, their properties can be tuned post-synthetically, by modifying the functionalities, this gives them an edge over previous materials with similar applications [8].

When co- or bridging ligands such as bipyridine, 1,10-phenanthroline, 4,4'-trimethylenedipyridine, imidazole are used as co-ligands alongside carboxylic acids, higher dimensionality and structural diversity of the resulting CP is obtainable as a result of their influence on the assembly process [9]. Several unique structural motifs and desirable functional properties, which cannot be obtained when only one type of ligand is used, can be conferred with the use of these N-donor ligands. Three zinc CPs were constructed with the use of 3,3'- thiodipropionic acid and three different pyridyl ligand [10]. CPs with dimensionalities ranging from 1D chain, 2D layer to 3D framework were obtained with the use of 1,3-bis(4-pyridyl)propane flexible ligands and 1,2-phenylenediacetic acid [11]. Different 5- functionalized isophthalate ligands were used alongside 4,4'- bipyridyl (bpy) and Zn(II) salt, for the synthesis of four CPs, the influence of the different functionalities on the structure of the CPs was investigated [12]. Most recently, we reported two Zn(II) coordination polymers constructed with 4-nitrobenzoate/ 4-biphenylcarboxylate and 4,4' -trimethylenedipyridine [13].

The presence of organic pollutants present in wastewater effluents is an environmental problem of concern, worldwide. They find their way into the ecosystem through natural and anthropogenic activities such as industrial or agricultural activities. Their mutagenic and carcinogenic potentials pose threat and harm to the aquatic environment and even human health [14]. Among these organic compounds are phenolic compounds. Phenols are classified among priority pollutants as a result of their harmful effects on organisms, even when present in concentrations as low as 0.005 $mgL^{-1}$ [15]. The wide use of phenols and chlorophenols as

wood preservatives, biocides, and precursors to the manufacture of herbicides, pesticides etc. has led to their abundance in wastewater effluents [16]. In addition, chlorophenols are also produced as by-products of water chlorination and wood bleaching using chlorine in pulp and paper industries [17]. Some of the effects of chlorophenols are chronic bronchitis, coughing and pulmonary defects [18]. The persistent and recalcitrant nature of these compounds has necessitated their remediation.

The technologies that have been used for remediation of phenolic compounds are membrane separation [19], ion exchange [20], biodegradation [21], oxidation [22] and adsorption [23]. Adsorption is most preferred due to its low operational cost, ease of operation and the possible reusability of the adsorbents [24]. Reports show that chitosan composites [25], zeolites [26], rattle seed pod [27], clay [28], activated carbon [29] etc. have been used for the adsorption of phenolic compounds from water. A relatively new class of adsorbents are the coordination polymers. They have high surface area and pore volume, high chemical stability, tunable properties and structures capable of strong interaction with target adsorbate through hydrogen bonding, electrostatic, π-π interaction and so on [30]. All these lead to the exhibition of high adsorption efficiency, high selectivity for the target molecule and satisfactory reusability for several adsorption cycles, thereby making them cost-effective [8]. There are several reports on the effective use of coordination polymers for the adsorption of phenolic compounds [31–35]. Our group previously reported the use of coordination polymers for environmental remediation [13,36–39].

This work also reports the efficiency of the Zn (II) CP in the adsorption of 2,4,6-trichlorophenol (TCP) (**Figure 1**) solution which is a representative organic compounds found in industrial effluents, especially pulp and paper industries. In addition, specific interactions that aided the adsorption of TCP were analysed. It is noteworthy that, to the best of our knowledge, no study in the use of CPs for the removal of TCP has been reported.

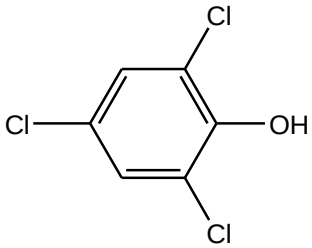


**Figure 1**: Structure of 2,4,6 -Trichlorophenol (TCP)

## 2. Experimental

### 2.1 Materials

$Zn(NO_3)_2 \cdot 6H_2O$ (98%), 4-hydroxybenzoic acid (99%), 4,4'- trimethylenedipyridine (98%), ethanol (99.9%), hydrochloric acid (37%), DMSO (99.7%), sodium hydroxide pellets (97%), and methyl orange dye were purchased from Sigma-Aldrich,Germany; 2,4,6-trichlorophenol (98%) from Alfa Aeser, England.

### 2.2 Preparation of $[Zn(hba)_2(tmdp)]_n$ (1):

$Zn(NO_3)_2 \cdot 6H_2O$ (0.296 g, 1 mmol) dissolved in 20 mL distilled water, 4-hydroxybenzoic acid (Hhba) (0.138 g, 1 mmol) in 10 mL ethanol and 4,4'- trimethylenedipyridine (0.199 g, 1 mmol) (tmdp) in 10 mL ethanol were mixed together and stirred at RT (~27°C) for 30 minutes. The beaker was then sealed and placed inside the oven at 80°C for 8 hours followed by slow evaporation of the resulting mixture. Colourless block-shaped crystals were formed after 3 days and filtered out of the solution. The synthetic pathway is shown on **Scheme S1**. Yield: 84%, Melting point: 224°C, Molecular weight: 537.87 g/mol, Anal. calc. for $C_{27}H_{24}N_2O_6Zn$: C, 60.29; H, 4.50; N, 5.21; Found: C, 60.14; H, 4.30; N, 5.02; IR peaks ($cm^{-1}$) 3447 (br), 2929(w), 1599 (s), 1543(w), 1431 (m), 1371 (s), 1250 (w), 682 (w), 437 (w).

### 2.3 Measurements

FT-IR measurements, in the range 4000-400 $cm^{-1}$, were performed with a Shimadzu 8400 spectrophotometer, Japan. The percentages of C, H, and N were obtained using a PerkinElmer PE-2400 CHN analyser. Thermal analysis was done with Mettler Toledo TGA/DSC 1-600 instrument. Powder X-ray diffraction measurements were collected on a Siemens D5000 diffractometer operating with Cu Kα1/2 radiation in flat-plate geometry. Single crystal X-ray analysis was done by placing a single crystal on a glass fibre with Fomblin oil, mounting it on an Xcalibur Gemini diffractometer with a Ruby CCD area detector and kept at 150(2) K when the data was collected. Using Olex2 [40], the structure was solved with the ShelXT [41] structure solution program using intrinsic phasing and refined with the ShelXL [42] refinement package using Least Squares minimization.

### 2.4 Adsorption experiment

To measure the adsorption capacity of (**1**), TCP concentrations of 20-100 ppm were prepared in deionised water. Adsorbent dosage of 0.01-0.05 g was added to 50 mL adsorbate solution

within the pH range of 2 to 12. The solution was shaken in an incubator shaker for 30-300 minutes, the solution temperature being within 298-333 K.

After the adsorption experiment, the spent adsorbent was separated from the supernatant using a centrifuge and subsequently decanting. The supernatant was analysed for TCP residual concentration by taking its absorbance at $\lambda_{max}$ of 269 nm, using a UV−Vis spectrophotometer. The dye removal capacity of one gram of (**1**) ($q_e$) was calculated using Equation S1:

For the reusability study, the used adsorbent was separated from the adsorbate solution, washed with deionised water and dried at $80^0$ C. This was subsequently shaken in 50 mL ethanol for one hour, and dried at room temperature. The percentage desorption was calculated using Equation S2.

### 2.5 Density functional theory (DFT) studies

Biovia Materials Studio 2018 was used for the computational studies. The determination of the most plausible starting positions to model the interaction between adsorbent and adsorbate, and the pre-optimization of geometry to ultra-fine quality was performed using the Forcite tool. Slight modification of literature methods was used to carry out the DFT studies using the $DMol^3$ module on the Forcite pre-optimized structures with convergence threshold parameters set at default (medium); energy = 0.00002, gradient = 0.004 and displacement = 0.005 [43,44]. The generalized gradient approximation (GGA) with Perdew-Burke-Ernzerhof (PBE) parametrization functional was applied with Grimme for DFT-D correction. Density functional semi-core pseudopotentials were fitted to all electrons with a double numerical plus (DNP) polarization basis set and a real-space orbital global cut-off of 4.4 Å. The studies were first carried out in gas phase before the conductor-like screening model (COSMO) was applied using water at a dielectric constant of 78.54. The sum of the energies of the adsorbent and adsorbate was subtracted from the total energy of the adsorbent/adsorbate dye cluster, to give the binding energies between the adsorbent and adsorbate (Equation S3).

## 3. Results and discussion

### 3.1 FT-IR spectra

Comparison of the FT-IR spectra of Hhba, tmdp and (**1**)**,** as shown in **Figure S1**, show some changes in the absorption bands due to the formation of a new entity.

IR spectrum of free ligand, Hhba, show broad ν(O-H) at 3390 $cm^{-1}$. This band disappeared in the spectrum of (**1**) indicating its involvement in the coordination with Zn(II) ion. The stretching frequencies of phenolic O-H and C-OH are at 3200 and 1250 $cm^{-1}$ respectively. The latter was not affected by the complexation, indicating that the phenolic OH did not coordinate to the metal [45].

Moreover, the C=O band of the ligand at 1720 $cm^{-1}$ disappeared in the spectrum of (**1**), indicating that the carboxylate oxygen coordinated to the metal ion. ν(C=N) band was situated at 1585 $cm^{-1}$ for tmdp, and was shifted to 1543 $cm^{-1}$ on compound (**1**) spectrum. Characteristic bands at the fingerprint region were also observed for the Zn-N and Zn-O vibrations at 682 $cm^{-1}$ and 437 $cm^{-1}$ respectively [46].

### 3.2 PXRD results

The simulated PXRD pattern of (**1**) was compared with that measured at room temperature (**Figure 2)**. Characteristic peaks of (**1**) were observed on both patterns, no extra peaks were found on the experimental pattern, indicating the phase purity of the bulk of (**1**)**.**

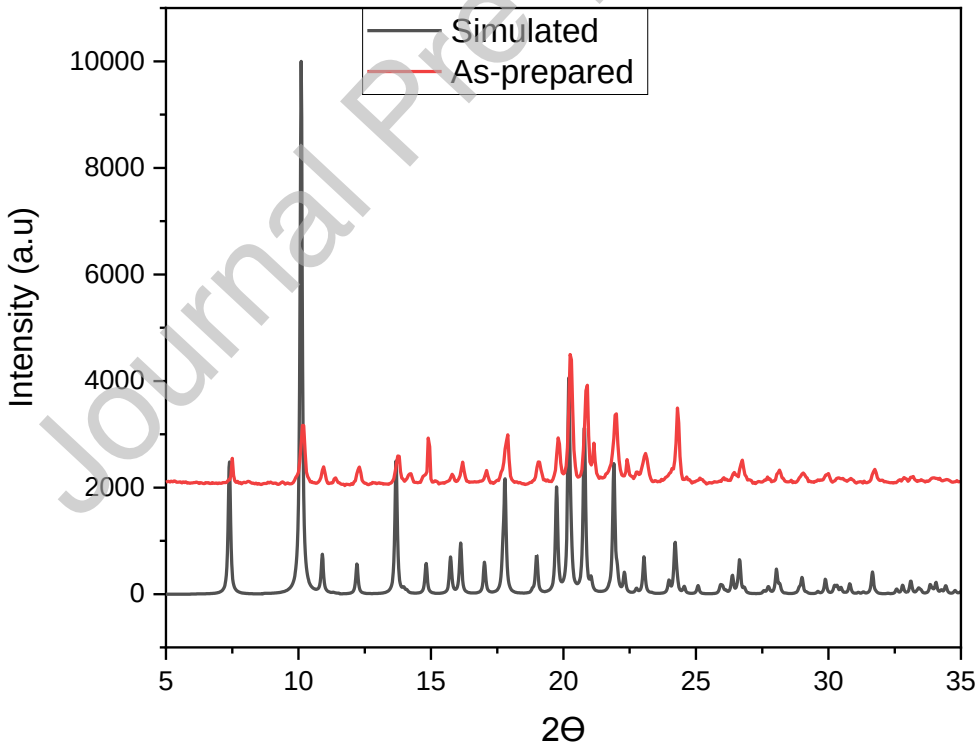


**Figure 2**: Simulated and as-prepared PXRD patterns of $[Zn(hba)_2(tmdp)_2]n$ (**1**)

### 3.3 Thermal analysis

Thermogravimetric analysis, in the range 25-800°C, was carried out and presented as shown in **Figure S2**. The TGA/DSC profile shows that the compound is thermally stable up to 200°C. Weight losses are observed to be in three steps. The first weight loss of 37.2% (calc.37%) within 200-260°C is attributed to the loss of tmdp ligand. The last two weight loss steps, each of 24% (calc. 25.46%), correspond to the loss both hba molecules: the first being in the range 260-300°C and the second in the range 454-510°C. 14% (calc.15.05%) of zinc oxide residue is seen to be stable up to 800°C. PXRD pattern of the product formed after the TGA analysis was obtained to confirm it was ZnO, as shown in **Figure S3**. The pattern was found to match that of zincite in the database (JCPDS No. 00-036-1451) [47]. The hkl values were included.

### 3.4 X-ray Crystallographic results

Compound **$[Zn(hba)_2(tmdp)]_n$ (1)** is built up of two *p*-hba and two tmdp molecules in a five-coordinate manner. It crystallizes in an orthorhombic system with space group F d d 2. The structure is shown in **Figure 3**. Crystal data and data collection summary are shown on **Table S1**.

The asymmetric unit is composed of a Zn (II) atom, two hba molecules and one tmdp molecule. There are two coordination modes of the p-hba ligand. One of the p-hba ligands coordinates monodentately with one carboxylate oxygen O16 while the second coordinates in a bidentate chelating mode with both carboxylate oxygen atoms O24 and O25. Atoms O16, O24, N3 and N13 reside at the corners of the basal plane, whereas the apical position is occupied by O25. However, the distance between O17 and Zn1 is 2.74 Å. This is considerably longer that the short Zn-O and Zn-N distances that define the coordination sphere and in fact more distant than carbon atoms, so cannot be considered a bonding distance. The square pyramidal geometry of the structure is slightly distorted, ascertained by the geometry index, $\tau$ of 0.041 ($\tau$ is 0 for a perfect square pyramidal and 1 for a perfect trigonal-bipyramidal geometry) [48]. The $\tau$ value of 0.041 indicates the deviation from perfect square pyradimal geometry. The significant deviation of the O-Zn-N from $90^o$ also supports this. Bond distances and angles around the metal ion are shown in **Table 1**. Two adjacent Zn(II) atoms are linked by the tmdp ligand to form 1D CPs, with the two carboxylate ligand molecules acting as pendants as shown in **Figures S4.**

The shortest bond distance between two zinc (II) centres is 9.440 **Å**. The bond distance of Zn1-N3 and Zn1-N13 are almost the same, around 2.0723 **Å** and compares favourably with those in literature [49–51] but the Zn-O bond distances range from 1.9574 to 2.4847 **Å**. Zn1-O24 and Zn1-O25 bond lengths are longer than Zn1-O16, this indicates a weaker ligand coordination ability of the chelating carboxylate than the monodentately coordinated carboxylate [52]. The similar bond lengths of C25-O24 (1.280 **Å**) and C25-O25 (1.230 **Å**) indicates that the bonding arrangement is delocalized, rather than localized single and double bonds. The methylene groups between the two pyridyl rings of tmdp ligand confer flexibility on it. The flexibility is confirmed by the significant dihedral angle of 179$^{o}$ between the planes of the two pyridyl rings. The plane of the carboxylic group of the hba ligand and that of the aromatic ring are far from being coplanar, as seen from the dihedral angle of 14.95$^{o}$ [53]. **Figure S5** shows that there are O-H…O intermolecular hydrogen bonds present, firstly between the free hydroxyl oxygen (O29) and a chelated oxygen atom (O25) of hba from adjacent structural units; and secondly between the free hydroxyl oxygen of another hba (O21) and the uncoordinated oxygen atom (O17) from adjacent structural units (**Table 2**). The compound is packed in a rib-like manner and the hydrogen bonds stabilize the supramolecular networks (**Figure S6**). The packing view of the unit cells for **1** is shown in **Figure 4**.

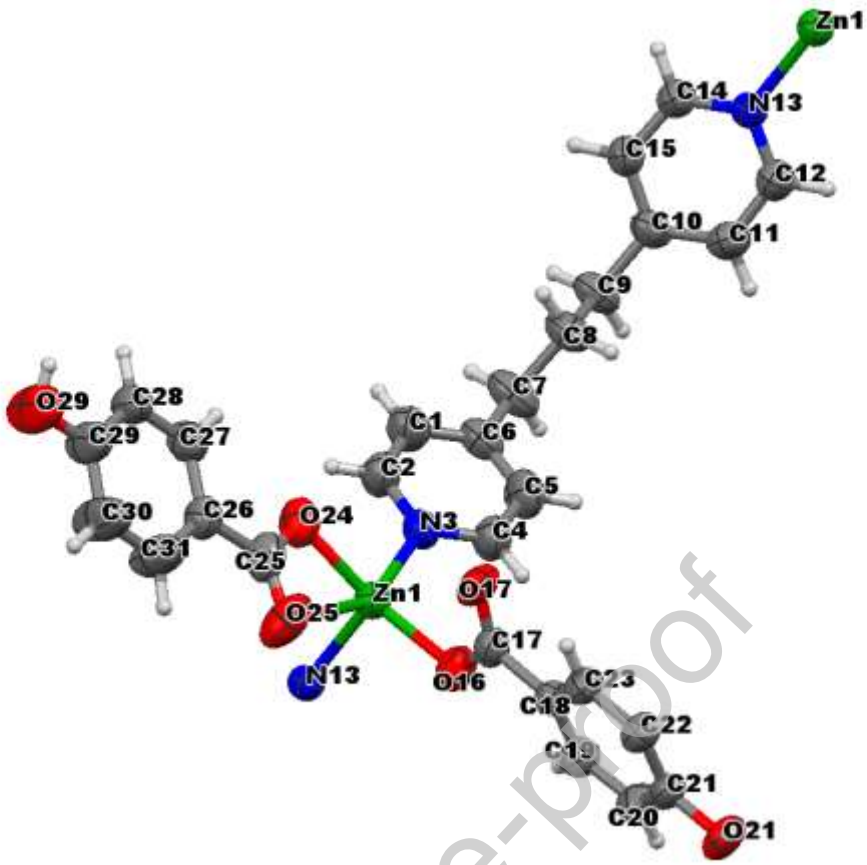


**Figure 3**. ORTEP diagram of $[Zn(hba)_2(tmdp)]_n$ (**1**) (Ellipsoids drawn at 50% probability level)

**Table** 1. Bond lengths and angles around Zn (II) in (**1**).

| **Bond length (Å)** | | **Bond angles (°)** | |
|---|---|---|---|
| Zn1-O16 | 1.957(3) | O16-Zn1-O24 | 147.8(1) |
| Zn1-O24 | 1.995(3) | O16-Zn1-N3 | 102.1(1) |
| Zn1-N3 | 2.072(3) | O16-Zn1-O25 | 101.9(1) |
| Zn1-O25 | 2.485(5) | O16-Zn1-N13 | 95.0(1) |
| Zn1-N13 | 2.075(3) | O24-Zn1-N3 | 93.7(1) |
| Zn1-O17 | 2.740(3) | O24-Zn1-O25 | 56.9(1) |
| | | O24-Zn1-N13 | 105.0(1) |
| | | N3-Zn1-O25 | 150.3(1) |
| | | N3-Zn1-N13 | 111.9(1) |
| | | O25-Zn1-N13 | 83.2(1) |

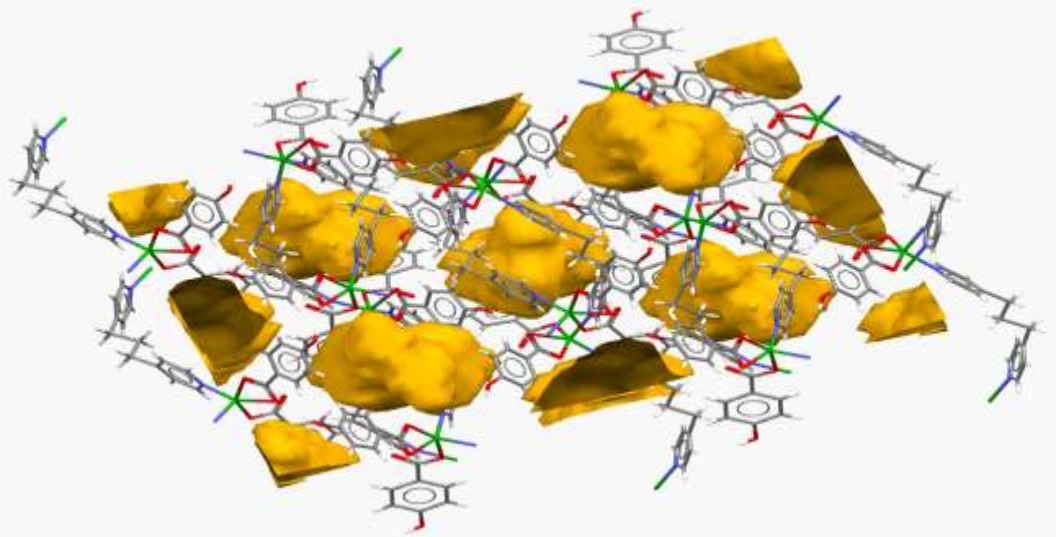

**Figure 4**. Packing view of (**1**) showing voids (represented in yellow)

**Table 2**: Selected hydrogen bond geometry in (**1**)

| D–H···A | D-H (Å) | H···A (Å) | D···A (Å) | D–H···A (°) |
|---|---|---|---|---|
| O21—H21···O17 | 0.82 | 1.83 | 2.649 (4) | 176 |
| O29—H29···O25 | 0.82 | 1.77 | 2.590 (7) | 176 |

Symmetry codes: (i) −x+3/4, y+1/4, z−1/4; (ii) −x+3/4, y−1/4, z+1/4



### 3.5 Adsorption studies

The adsorption of TCP from aqueous medium using (**1**) and a previously reported analogous Zn (II) coordination polymer ($[Zn(biphen)_2(tmdp)]_n$ (biphen= 4-biphenylcarboxylic acid, tmdp= 4,4'- trimethylenedipyridine) was investigated. The reported procedure [13] was used for the synthesis of $[Zn(biphen)_2(tmdp)]_n$, its structure is given in **Figure 5**.

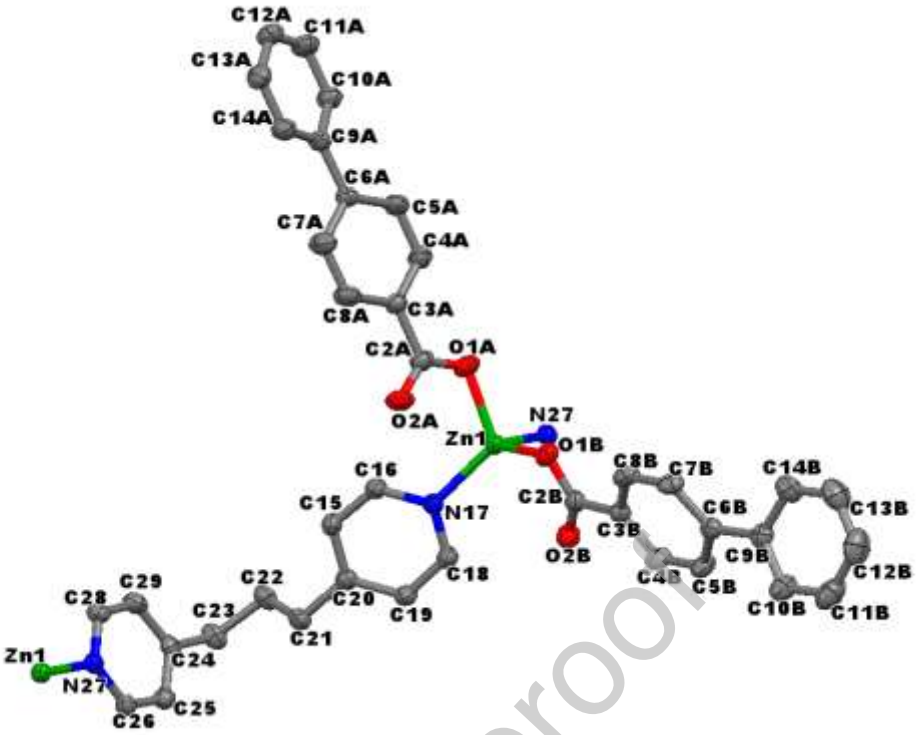


**Figure 5**: Crystal structure of $[Zn(biphen)_2(tmdp)]_n$ (Hydrogen atoms omitted for clarity)[13]

With a starting adsorbate concentration of 100 mg/L, after 300 minutes of stirring, $Zn(biphen)_2(tmdp)]_n$ had an adsorption capacity of 32.60 mg/g in contrast to 207.8 mg/g obtainable with the use of **(1).** The lower adsorption capacity of $[Zn(biphen)_2(tmdp)]n$ than that of **(1)** could be attributed to the steric hindrance caused by the bulky nature of the biphen moieties intercalated into the voids created from its packing, as shown in **Figure S7**. This justifies the void volume of the channels of (**1**) and $[Zn(biphen)_2(tmdp)]_n$ calculated using PLATON (1295.93 $Å^3$ and 141.00 $Å^3$ respectively.

The excellent uptake of TCP by (**1**) motivated its eventual use for the adsorption process and some operational parameters were optimized.

### 3.5.1 Optimization of operational parameters

In optimizing the pH for the adsorption process, the effect of pH on chlorophenol species distribution was investigated using the Equation S4 [54]. The pKa is 6.2 for TCP. Using the equation, it was determined that as the pH increases, the fraction of the unionized species of TCP reduces and that of the ionized species increases. The pHpzc for (**1**) was found to be 7.5 (**Figure S8**). In the pH range 2-6, as shown in **Figure 6,** the adsorption capacity of (**1**) for TCP was almost constant but the highest adsorption efficiency was observed at pH 6 (202 mg/g). Moreover, at higher pH, the surface of (**1**) is negatively charged resulting in reduced

electrostatic repulsion between negatively charged surface of (**1**) and ionised TCP species [55] and ultimately reduced adsorption. Adsorption of a certain amount of TCP was still possible in the basic condition, indicating that other mechanisms apart from electrostatic interaction might have taken effect.

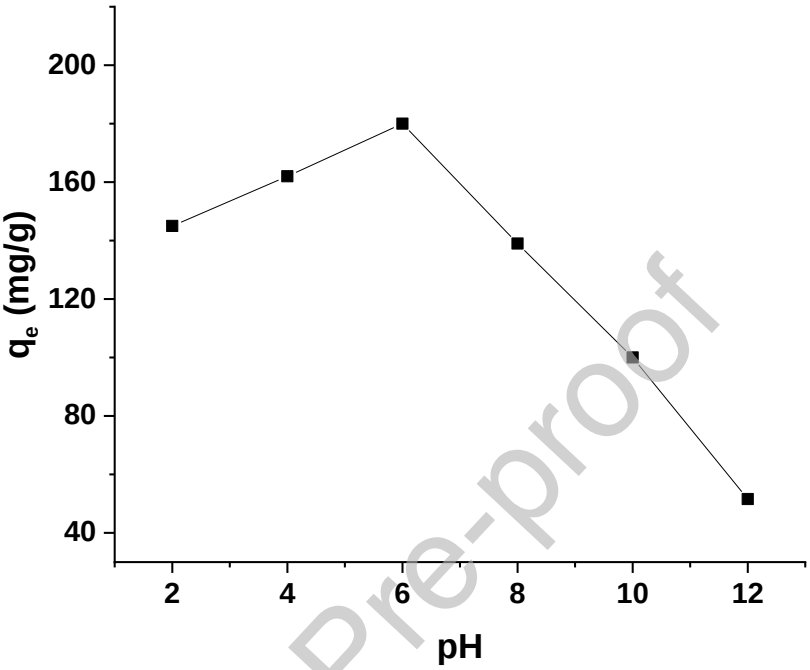


**Figure 6**: Effect of pH on the adsorption of TCP on (**1**)

Various amounts of (**1**) (0.01 to 0.05 g) were used for the adsorption process to investigate the maximum uptake with 50 mL of 100 mg/L of TCP. From **Figure S9**, the adsorbent dosage with the maximum adsorption capacity is 0.03 g. Therefore, 0.03 g adsorbent dosage was taken as the optimum.

The experiments were performed in the range 298 – 333 K for the optimization of the solution temperature (**Figure S10a**). Maximum adsorption capacities for TCP by (**1**) was obtained at 298 K but dropped when the temperature was increased. This indicates the exothermic nature of the adsorption processes. The Van't Hoff plot for the adsorption process is given in **Figure S10b** and **Table 3** shows the calculated values of the parameters $\Delta H$, $\Delta S$ and $\Delta G$ for the adsorption processes.

**Table 3**: Thermodynamic parameters of the adsorption of TCP on (1).

| Temp ( K ) | ΔG (kJ $mol^{-1}$) | ΔH (kJ $mol^{-1}$) | ΔS ($Jmol^{-1}K^{-1}$) |
|---|---|---|---|
| 298 | -6.89 | -32.60 | -86.20 |
| 313 | -5.68 | | |
| 323 | -4.82 | | |
| 333 | -3.96 | | |

When the value of ΔH is lesser than 40 kJ $mol^{-1}$, the adsorption process is physisorption [56]. The calculated value of ΔH indicates physisorption processes. The ΔG values for the adsorption process are less than zero indicating that it is spontaneous and feasible. The negative value of Δ*S* indicates a high degree of order during the adsorption process [57].

The optimization of the TCP concentration was done by using an adsorbent dosage of 0.03 g in 50 mL of different concentrations of TCP in the range (20-100 mg/L) at 298 K and pH 6 for 120 minutes. The uptake of TCP by (**1**) as illustrated in **Figure S11,** increases from 30.7 to 202.8 mg/L when the initial concentration of TCP was raised from 20 to 100 mg/L. This is due to the fact that easily accessible large vacant sites were available for adsorption up to a certain point after which they became saturated [58].

The optimization of the contact time on the uptake of TCP by (**1**) was studied by using an adsorbent dosage of 0.03 g in 50 mL of 100 mg/L of TCP at 298 K and pH 6 for a time range of 30-300 minutes. There was rapid adsorption in the first 180 min (**Figure S12)**, after which no obvious increase was observed. This is as a result of less sites available to be occupied [59].

### 3.5.2 Adsorption Isotherm

Langmuir, Freundlich, Temkin and Dubinin-Radushkevich (D-R) models were used for the isotherm studies. The equations are given in **Equations S5-8** respectively.

From the results of the isotherm plots shown in **Figures S13a-d** and **Table S2**, the better fit of Freundlich model than Langmuir model, as depicted by their $R^2$ values, indicate multi linear adsorption and the heterogeneity of the adsorbent surface [60]. The high $R^2$ of the Temkin isotherm plot shows the linear dependence of heat of adsorption at low or medium coverages and also repulsion between adsorbate species or to intrinsic surface heterogeneity

(Kalavath *et al.*, 2005). The mean sorption energy, E (**Equation S9**), obtained is 0.14 kJ/mol, indicating a physisorption process.

### 3.5.3 Adsorption Kinetics

Pseudo-first-order and pseudo-second-order models were used for the kinetics studies. The mass transfer mechanisms were analysed using Intraparticle, Bangham and Boyd diffusion models. The equations are given in **Equations S10-14** respectively.

From the results of the kinetic plots shown in **Figures S14a, b** and **Table 4,** the $R^2$ value for pseudo second order is higher than pseudo first order model, therefore, the sorption process follows pseudo second order. This is supported by the closeness of the adsorption capacity obtained from the pseudo second order to the experimental adsorption capacity.

The non-zero and multilinearity of the straight line obtained from the intraparticle diffusion model plot (**Figure S14c**) shows the contribution of other mechanisms to the rate-limiting step, the first, second and third lines representing boundary layer effect, intraparticle and pore-adsorption respectively [62]. The Bangham diffusion model plot (**Figure S14d**) supports the involvement of other rate-controlling steps, with boundary layer diffusion, in the sorption process. The straight line of Boyd plot (**Figure S14e**), which does not pass through the origin is an indication of a film-diffusion controlled process [63]. The kinetic data primarily signifies chemisorption and monolayer adsorption, therefore, CP can accommodate approximately one molecule of TCP per zinc site, hence absorbed amount is likely to form 1:1 TCP-CP (**1**) adduct.



**Table 4**: Kinetics parameters of the adsorption of TCP on (1)

| **Kinetic model** | **Parameter** | **Values** |
|---|---|---|
| | $Q_e$ exp (mg/g) | 207.8 |
| Pseudo-first order | $K_1$ ($min^{-1}$) | 0.0298 |
| | $Q_e$ (mg/g) | 514 |
| | $R^2$ | 0.9204 |
| Pseudo-second order | $K_2$ (mg/gmin) | $1.02 \times 10^{-4}$ |
| | $Q_e$ (mg/g) | 241 |

| | | |
|---|---|---|
| | $R^2$ | 0.9893 |
| Intraparticle diffusion | C(mg/g) | 9.1 |
| | $K_p$ (mg/g(min)$^{1/2}$) | 16.74 |
| | $R^2$ | 0.9986 |
| Bangham | α | 0.55 |
| | $K_0$(g) | 11.17 |
| | $R^2$ | 0.9321 |
| Boyd | B (sec$^{-1}$) | 0.0298 |
| | $R^2$ | 0.9203 |

### 3.5.6 Reusability study

Probable reusability of the adsorbent was investigated to ascertain its viability for industrial applications. This is shown in **Figure 7 and Table S3.** After three adsorption-desorption cycle, only a small decrease in the adsorption capacity of (**1**) was observed. The percentage of adsorbed TCP on (**1**) decreased by only 2.79% after the third use.

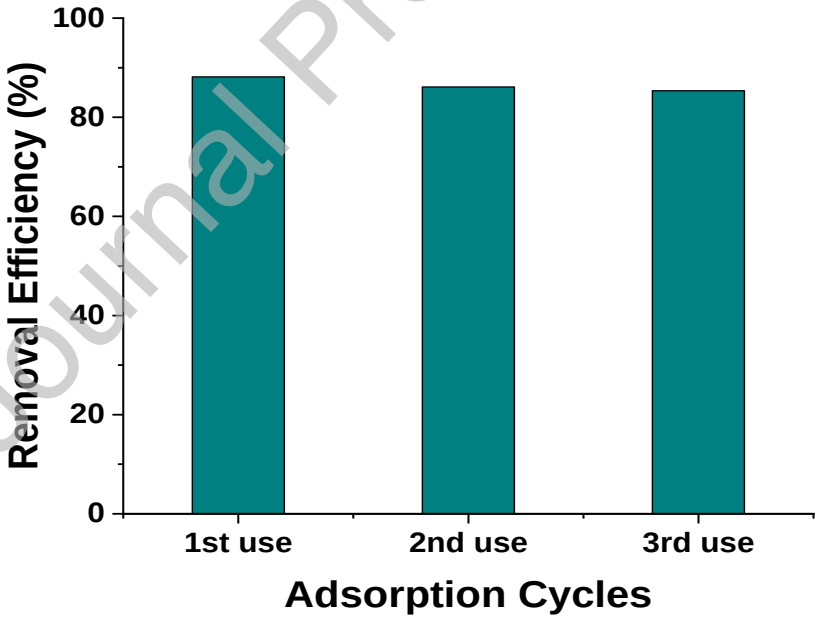


**Figure 7**: Removal efficiency of (**1**) after three adsorption-desorption cycles of TCP

FT-IR and PXRD analyses were performed on the spent adsorbent after the adsorption process. The maintenance of the structure after adsorption was ascertained by the PXRD analysis (**Figure 8)**. There is no disappearance of existing peaks or appearance of new peaks, only decrease in the intensity of the peaks was observed.

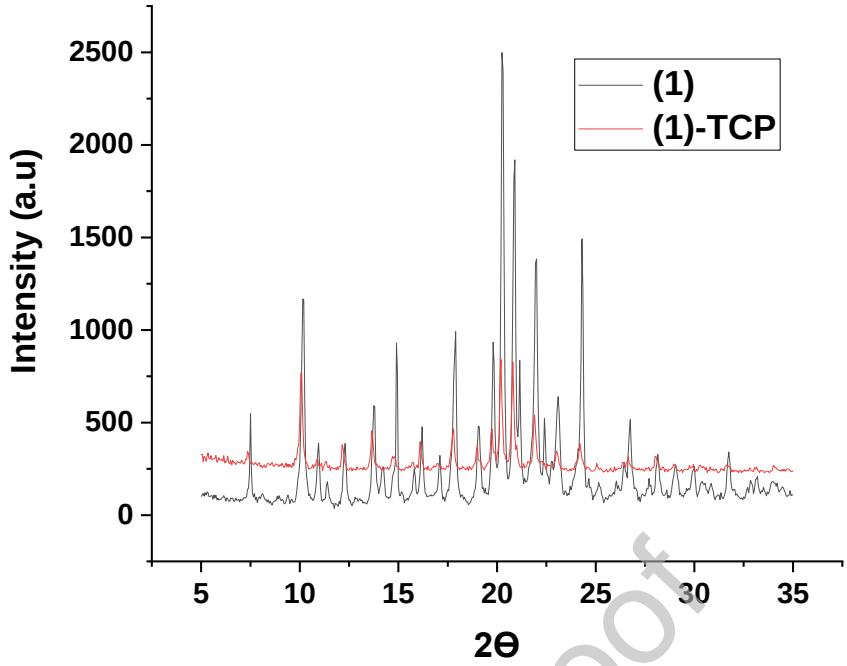


**Figure 8**: PXRD patterns of (**1**)before and after adsorption of TCP

The FT-IR spectra of (**1**) and (**1**)-TCP (after TCP adsorption) were compared as shown in **Figure 9**. After the adsorption of TCP, the breadth of the phenolic O-H seen around 3200 $cm^{-1}$ band changed (as shown with the oval shapes) and also, its center was shifted, indicating the interactions between the phenolic O-H groups of **(1)** and TCP. The intensity of the $–COO^-$ peak at 1543 $cm^{-1}$ changed after adsorption of TCP showing that it was involved in the adsorption of TCP. Other information from the comparison of the IR spectra is the presence of new bands at 1220 and 704 $cm^{-1}$ on **(1)**-TCP which is absent on **(1)** and can be related to the phenolic C-O and C—Cl stretching vibration of TCP, respectively. In like manner, new bands seen around 1431-1461 $cm^{-1}$ on **(1)**-TCP are attributed to the deformation vibration of hydroxyl groups and the vibrations of C—H [56]. In addition, it is believed that the pi-pi stacking interactions between the aromatic rings of TCP and **(1)** can also be beneficial to the adsorption of TCP. This was suggested for the adsorption of 2,4-dichlorophenol and the imidazolium ring of cyclodextrin-ionic liquid polymer [64]. A possible mechanism has been proposed using the DFT studies as discussed in **section 3.5.7**.

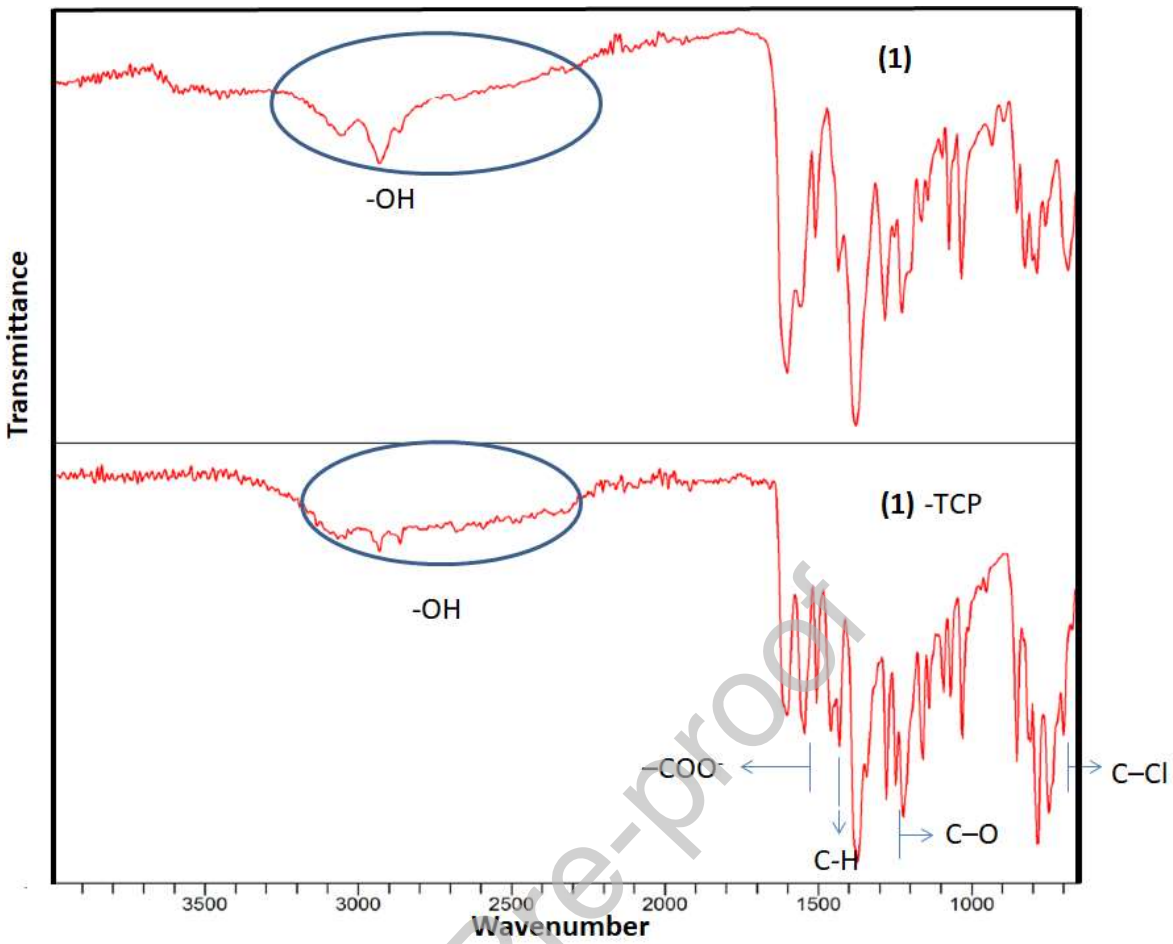


**Figure 9**: FT-IR spectra of **(1)** before and after adsorption of TCP



### 3.5.7 DFT Studiess

To gain insight into CP unit (**1**) interaction with TCP through the formation of adduct, DFT calculations was employed due to the observed 2$^{nd}$ order kinetic data. Pre-optimization of the structures was done using Biovia Forcite.

The effect of pH in the adsorption of TCP on (**1**) was studied theoretically by modelling the ionized forms of the starting materials and the clusters under the same conditions. Binding energies were also calculated. The neutral model of TCP was more stable based on the SCF and binding energies (**Table 5** and **Figure 10**).

The total energies of possible starting positions in the interaction of (**1**) and TCP were calculated and it was deduced that the lowest energies were possessed by the clusters where the TCP molecules presented pi-pi interactions with the aromatic rings (4-hydroxybenzoic

acid of CP and -OH of TCP pointing towards the Zn centre. The study clearly showed that dispersion forces, particularly pi-pi interactions, electron donating properties of –OH play pivotal roles, thus responsible for CP and TCP interactions.

The π-π interaction between the phenolic compound and the adsorbent, which is said to have contributed to the adsorption process, has been reported for the adsorption of other phenolic compounds by different adsorbents.

A cobalt coordination polymer composite TMU-10@Graphene oxide was reported to have a high adsorption capacity as a result of the π-π interaction contributed by the aromatic rings of the composite and the phenolic ring [65]. In the adsorption of phenol and para-nitrophenol using activated carbon from cauliflower waste, the π-π interaction between aromatic rings of phenols and adsorbents surface was proposed to have influenced the adsorption efficiency [66]. Hydrogen bond and also π-π interactions were said to be the driving force for the adsorption of PNP on the coordination polymer MIL-68(Al) and reduced graphene oxide (MA/RG) composite [67].

The BE was calculated to be -14.81 Ha for neutral system. The BE between deprotonated (anionic phenolate) TCP and CP **(1)** was -15.39 Ha, which slightly lower than the neutral system. However, this did not translate to higher adsorption of TCP from experimental data, thus, suggesting that –OH group of TCP influences the interactions responsible for adduct formation, furthermore electronic properties respond more to changes in pH.

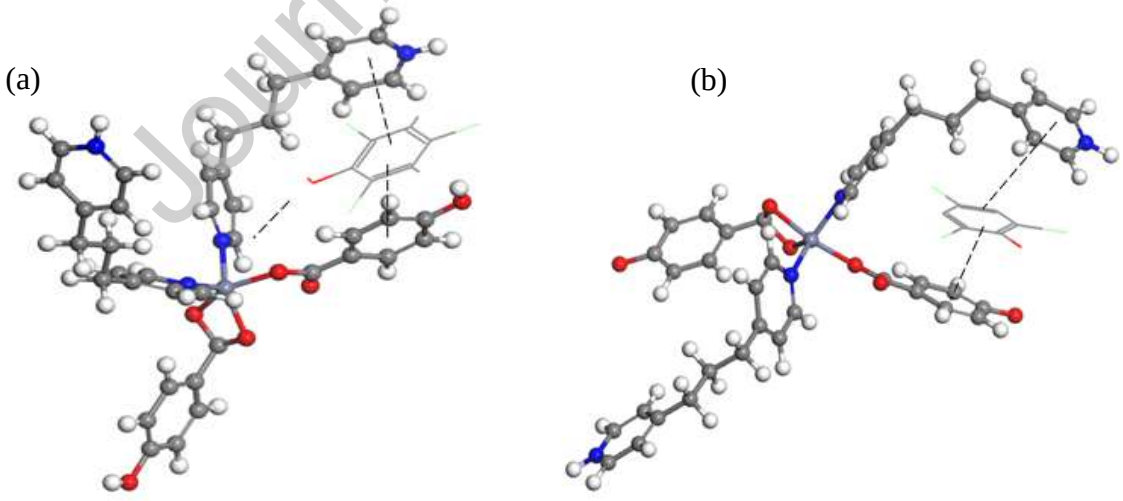


**Figure 10**. Biovia Materials Studio 2018 DMol$^3$ modelled structures showing adsorption of TCP on (**1**) (a) neutral model and (b) anionic model.

**Table 5. Energies of the adsorbents, adsorbates and their clusters; and calculations for binding energy (BE)**

| | Gibbs free | SCF (Ha) | BE (Ha) |
|---|---|---|---|
| **(1)** anionic | 348.48 | -3995.68 | -17.64 |
| **(1)** neutral | 392.98 | -3996.22 | -17.19 |
| TCP anionic | 16.09 | -1684.92 | -2.25 |
| TCP neutral | 24.51 | -1690.53 | -2.38 |
| **(1)** anionic – TCP (cluster) | 161.51 | -5685.96 | -26.22 |
| **(1)** stand – TCP (cluster) | 172.44 | -5686.58 | -25.84 |
| (1) anionic + TCP (sum) | 364.58 | -2310.76 | -15.39 |
| (1) neutral + TCP (sum) | 417.49 | -2305.69 | -14.81 |
| ionic cluster – sum | -203.07 | -3375.19 | -10.82 |
| neutral cluster – sum | -245.05 | -3380.89 | -11.03 |

However, for further assessment of the removal capacity of (1), its phenol-removal efficiency was tested. The adsorption capacity of phenol was 157.6 mg/g. The result obtained could also be attributed to the π-π interaction between aromatic rings of phenol and (1). The slightly lower adsorption capacity than that of TCP could be as a result of the higher water solubility of phenol compared to TCP (83 and 0.8 g/L respectively at 20°C) [31].

### 3.5.8 Comparison of TCP-removal efficiency of (1) to other reported adsorbents

A range of adsorbents have also been tested for the removal of TCP from water. **Table 6** shows the comparison of the adsorption capacities of some of them, for the adsorptive uptake of TCP. However, for economical and industrial application, a holistic consideration of other factors aside from the adsorption capacities, is needed. Such factors include the need for input of heat energy and the regeneration of the spent adsorbent. From the study of the effect of temperature on the adsorption process, compound **(1)** was found to give the maximum adsorption capacity at ambient temperature, there was no need for the application of heat

energy to maximise the adsorption capacity. Also, the favorable reusability of **(1)** makes it an economical adsorbent for TCP removal from wastewater compared to previously reported adsorbents.

**Table 6**: Comparison of adsorption capacities of previously used adsorbents for TCP uptake

| Adsorbent | Qm (mg/g) | Effect of temperature | Reusability cycle | References |
|---|---|---|---|---|
| Activated carbon prepared from coconut shell | 112.35 | - | Yes | [68] |
| Activated clay | 123.46 | Exothermic | - | [60] |
| Activated carbon prepared from coconut husk | 191.73 | - | - | [69] |
| Activated carbon prepared from oil palm empty fruit bunch | 210.8 | Endothermic | - | [70] |
| Activated carbon prepared from oil palm empty fruit bunch | 168.89 | - | - | [71] |
| Chitosan/-$Fe_2O_3$/fly-ash composites | 172.4 | Endothermic | Yes | [25] |
| Chitosan | 27.6 | - | - | [72] |
| Albizia lebbeck (Rattle Seed) Pod | 6.80 | - | - | [27] |
| Activated Carbon prepared from Flamboyant pod bark | 37.64 | Exothermic | - | [73] |
| $[Zn(hba)_2(tmdp)]_n$ | 207.8 | Exothermic | Yes | This work |

### 3.6 Conclusions

A zinc (II) coordination polymer, $[Zn(hba)_2(tmdp)]_n$ **(1)** was synthesized from zinc nitrate hexahydrate, 4-hydroxybenzoic acid and 4,4'- trimethylenedipyridine. The removal of 2,4,6-trichlorophenol from aqueous solution was also reported. Compound **(1)** is a 1D coordination polymer and it adopts a square pyramidal arrangement. Freundlich isotherm and pseudo

second order kinetic models were found to fit best. The adsorption capacity reached 207.8 mg/g for TCP. The adsorption process was found to be aided by electrostatic and pi-pi interactions. Therefore, this work presents a novel material for environmental remediation applications.

**Supplementary data**

CCDC **1954757** contains the crystallographic data of $[Zn(hba)_2(tmdp)]_n$ **(1)**. This can be obtained from The Cambridge Crystallographic Data Centre via www.ccdc.cam.ac.uk/structures.

**Conflict of Interest**

The authors declare no conflict of interests.

## Credit Author Statement

| | |
|---|---|
| **A. C. Oladipo, V.T.Olayemi, O.B.Akpor** - | Conceptualization, Methodology, Data curation, Writing Original Draft. |
| **A. C. Tella, R. I. Walton, A.S. Ogunlaja** - | Formal analysis,Supervision,Funding Acquisition , Writing and Editing. |
| **A.S. Ogunlaja , H. S. Clayton, T.O. Dembaremba, A .C. Tella** | DFT studies, Supervision, Review and Editing |
| | Supervision, Writing and Editing. |
| **G.Y.Clarkson and R.I. WaIton** | X-ray Structure analysis and Discussion |

**Acknowledgement**

A.C. Oladipo is grateful to the Royal Society of Chemistry for the Researchers' Mobility Grant award, and also to University of Warwick, UK, for the facilities for the analysis of the compounds. The authors thank the Center for High Performance Computing (CHPC), Cape Town, South Africa for providing the platform for DFT studies using Biovia Materials Studio 2018.

**References**

[1] A. Beheshti, F. Panahi, P. Mayer, H. Motamedi, E. Parisi, R. Centore, Synthesis, structural characterization, antibacterial activity and selective dye adsorption of silver (I)-based coordination polymers by tuning spacer length and binding mode of chromate anion, J. Solid State Chem. 287 (2020) 121322. https://doi.org/10.1016/j.jssc.2020.121322.

[2] M.I. Rogovoy, A.S. Berezin, Y.N. Kozlova, D.G. Samsonenko, A.V. Artem'ev, A layered Ag(I)-based coordination polymer showing sky-blue luminescence and antibacterial activity, Inorg. Chem. Commum.Chem. Commun. 108 (2009) 107513.

[3] A. Biswas, M.B. Kim, S.Y. Kim, T.U. Yoon, S.I. Kim, Y.S. Bae, A novel 3-D microporous magnesium-based metal–organic framework with open metal sites, RSC Adv. 6 (2016) 81485–81490.

[4] M. Leroux, N. Mercier, M. Allain, M.-C. Dul, J. Dittmer, A.H. Kassiba, J.-P. Bellat, G. Weber, I. Bezverkhyy, Porous Coordination Polymer Based on Bipyridinium Carboxylate Linkers with High and Reversible Ammonia Uptake, Inorg. Chem. 55 (2016) 8587–8594.

[5] A. Lopez, J. Liu, Self- Assembly of Nucleobase, Nucleoside and Nucleotide Coordination Polymers: From Synthesis to Applications, Chem. Nano. Mat. 3 (2017) 670–684.

[6] I.R. Colinas, M.D. Rojas-Andrade, I. Chakraborty, S.R.J. Oliver, Two structurally diverse Zn-based coordination polymers with excellent antibacterial activity, CrystEngComm. 20 (2018) 3353–3362. https://doi.org/10.1039/c8ce00394g.

[7] S. Kulovi, S. Dalbera, S.K. Dey, S. Maiti, H. Puschmann, E. Zangrando, S. Dalai, S. Kulovi, S. Dalbera, S.K. Dey, S. Maiti, H. Puschmann, E. Zangrando, S. Dalai, ChemistrySelect. 3 (2018) 5233–5242.

[8] G.I. Dzhardimalieva, R.K. Baimuratova, E.I. Knerelman, G.I. Davydova, S.E. Kudaibergenov, O. V. Kharissova, V.A. Zhinzhilo, I.E. Uflyand, Synthesis of

copper(II) trimesinate coordination polymer and its use as a sorbent for organic dyes and a precursor for nanostructured material, Polymers (Basel). 12 (2020) 1024. https://doi.org/10.3390/POLYM12051024.

[9] Q. Yang, S. Ren, Y. Hao, Q. Zhao, Z. Chen, H. Zheng, Cyclopentaneteracarboxylic Metal-Organic Frameworks: Tuning the Distance between Layers and Pore Structures with N-Ligands, Inorg. Chem. 55 (2016) 4951–4957. https://doi.org/10.1021/acs.inorgchem.5b02340.

[10] H.J. Cheng, Y.L. Shen, S.Y. Zhang, H.W. Ji, W.Y. Yin, K. Li, R.X. Yuan, Three coordination polymers constructed with zinc(II), 3,3′-thiodipropionic acid, and bipyridyl ligands: Syntheses, crystal structures and luminescent properties, Zeitschrift Fur Anorg. Und Allg. Chemie. 641 (2015) 1575–1580. https://doi.org/10.1002/zaac.201500167.

[11] L.Y. Xin, G.Z. Liu, L.Y. Wang, New coordination polymers from 1D chain, 2D layer to 3D framework constructed from 1,2-phenylenediacetic acid and 1,3-bis(4-pyridyl)propane flexible ligands, J. Solid State Chem. 184 (2011) 1387–1392. https://doi.org/10.1016/j.jssc.2011.04.002.

[12] T. Wang, R.R. Zhu, X.F. Zhang, T. Yan, Q. Wang, J. Feng, J. Zhou, L. Du, Q.H. Zhao, Assembly of a series of zinc coordination polymers based on 5-functionalized isophthalic acids and dipyridyl, RSC Adv. 8 (2018) 7428–7437. https://doi.org/10.1039/c7ra12874f.

[13] A.C. Tella, A.C. Oladipo, V.O. Adimula, V.T. Olayemi, T.O. Dembaremba, A.S. Ogunlaja, G.J. Clarkson, R.I. Walton, Synthesis and Crystal Structures of Zinc(II) coordination polymers of trimethylenedipyridine (tmdp), 4-nitrobenzoic (Hnba) and 4-biphenylcarboxylic acid (Hbiphen) for adsorptive removal of methyl orange from aqueous solution, Polyhedron. 192 (2020) 114819. https://doi.org/10.1016/j.poly.2020.114819.

[14] Y. qiong Wang, B. Gu, W. lin Xu, Electro-catalytic degradation of phenol on several metal-oxide anodes, J. Hazard. Mater. 162 (2009) 1159–1164. https://doi.org/10.1016/j.jhazmat.2008.05.164.

[15] M.W. Jung, K.H. Ahn, Y. Lee, K.P. Kim, J.S. Rhee, J.T. Park, K.J. Paeng, Adsorption characteristics of phenol and chlorophenols on granular activated carbons (GAC), Microchem. J. 70 (2001) 123–131. https://doi.org/10.1016/S0026-265X(01)00109-6.

[16] A. Sinha, P. Bose, Interaction of 2,4,6-trichlorophenol with high carbon iron filings: Reaction and sorption mechanisms, J. Hazard. Mater. 164 (2009) 301–309.

https://doi.org/10.1016/j.jhazmat.2008.08.005.

[17] L.J. Graham, J.E. Atwater, G.N. Jovanovic, Chlorophenol dehalogenation in a magnetically stabilized fluidized bed reactor, AICHE J. 52 (2006) 1083–1093.

[18] R. Gao, J. Wang, Effects of pH and temperature on isotherm parameters of chlorophenols biosorption to anaerobic granular sludge, J. Hazard. Mater. 145 (2007) 398–403.

[19] M. Xiao, J. Zhou, Y. Tan, A. Zhang, Y. Xia, L. Ji, Treatment of highly-concentrated phenol wastewater with an extractive membrane reactor using silicone rubber, Desalination. 195 (2006) 281–293.

[20] M. Caetano, C. Valderrama, A. Farran, J.L. Cortina, Phenol removal from aqueous solution by adsorption and ion exchange mechanisms onto polymeric resins., J. Colloid. Interf. Sci. 338 (2009) 402–409.

[21] N.K. Sharma, L. Philip, Effect of cyanide on phenolics and aromatic hydrocarbons biodegradation under anaerobic and anoxic conditions., Chem. Eng. J. 256 (2014) 255–267.

[22] J. Jiang, Y. Gao, S.Y. Pang, X.T. Lu, Y. Zhou, J. Ma, Q. Wang, Understanding the role of manganese dioxide in the oxidation of phenolic compounds by aqueous permanganate., Env. Sci. Technol. 49 (2015) 520–528.

[23] D. Zhang, P. Huo, W. Liu, Behavior of phenol adsorption on thermal modified activated carbon, Chinese J. Chem. Eng. 24 (2016) 446–452.

[24] A.. Dada, J.. Ojediran, A.. Olalekan, Sorption of Pb2+ from aqueous solution unto modified rice husk: isotherms studies., Adv Phys Chem. 1 (2013) 1–8.

[25] J. Pan, H. Yao, X.X. Li, B. Wang, P. Huo, W. Xu, H. Ou, Y. Yan, Synthesis of chitosan/γ-Fe2O3/fly-ash-cenospheres composites for the fast removal of bisphenol A and 2,4,6-trichlorophenol from aqueous solutions, J. Hazard. Mater. 190 (2011) 276–284. https://doi.org/10.1016/j.jhazmat.2011.03.046.

[26] Y. Zhang, R.G. Mancke, M. Sabelfeld, S.U. Geißen, Adsorption of trichlorophenol on zeolite and adsorbent regeneration with ozone, J. Hazard. Mater. 271 (2014) 178–184. https://doi.org/10.1016/j.jhazmat.2014.02.020.

[27] A.H. Alabi, A.I. Buhari-Alade, F.O. Sholaru, R.F. Awoyemi, Biosorption of Phenols and Dyes on Albizia lebbeck (Rattle Seed) Pod: Equilibrium and Kinetic Studies, CRDEEP Journals Int. J. Environ. Sci. Alimoh H. Alabi et. Al. 5 (2015) 154–165. www.crdeepjournal.org/ijes.

[28] L. Tabana, S. Tichapondwa, F. Labuschagne, Adsorption of Phenol from Wastewater

Using Calcined Magnesium-Zinc-Aluminium Layered Double Hydroxide Clay, (2020).

[29] B. Xie, J. Qin, S. Wang, X. Li, H. Sun, W. Chen, Adsorption of Phenol on Commercial Activated Carbons : Modelling and Interpretation, (2020) 1–13. https://doi.org/10.3390/ijerph17030789.

[30] Z. Hasan, S.H. Jhung, Removal of hazardous organics from water using metal-organic frameworks (MOFs): Plausible mechanisms for selective adsorptions, J. Hazard. Mater. 283 (2015) 329–339. https://doi.org/10.1016/j.jhazmat.2014.09.046.

[31] B. Liu, F. Yang, Y. Zou, Y. Peng, Adsorption of phenol and p -nitrophenol from aqueous solutions on metal-organic frameworks: Effect of hydrogen bonding, J. Chem. Eng. Data. 59 (2014) 1476–1482. https://doi.org/10.1021/je4010239.

[32] K.Y. Andrew Lin, Y.T. Hsieh, Copper-based metal organic framework (MOF), HKUST-1, as an efficient adsorbent to remove p-nitrophenol from water, J. Taiwan Inst. Chem. Eng. 50 (2015) 223–228. https://doi.org/10.1016/j.jtice.2014.12.008.

[33] M. Maes, S. Schouteden, L. Alaerts, D. Depla, D.E. De Vos, Extracting organic contaminants from water using the metal-organic framework CrIII(OH)·{O2C-C6H 4-CO2}, Phys. Chem. Chem. Phys. 13 (2011) 5587–5589. https://doi.org/10.1039/c0cp01703e.

[34] E. Wu, Y. Li, Q. Huang, Z. Yang, A. Wei, Q. Hu, Laccase immobilization on amino-functionalized magnetic metal organic framework for phenolic compound removal, Chemosphere. 233 (2019) 327–335. https://doi.org/10.1016/j.chemosphere.2019.05.150.

[35] T. Boontongto, R. Burakham, Evaluation of metal-organic framework NH2-MIL-101(Fe) as an efficient sorbent for dispersive micro-solid phase extraction of phenolic pollutants in environmental water samples, Heliyon. 5 (2019). https://doi.org/10.1016/j.heliyon.2019.e02848.

[36] A.C. Tella, S.O. Owalude, S.J. Olatunji, S.O. Oloyede, A.S. Ogunlaja, S.A. Bourne, Synthesis, crystal structure and desulfurization properties of zig-zag 1D coordination polymer of copper(II) containing 4-methoxybenzoic acid ligand, J. Sulfur Chem. 39 (2018) 588–606. https://doi.org/10.1080/17415993.2018.1489808.

[37] A.C. Oladipo, A.C. Tella, V.T. Olayemi, V.O. Adimula, T.O. Dembaremba, A.S. Ogunlaja, H.S. Clayton, G.J. Clarkson, R.I. Walton, Synthesis, structural and DFT investigation of Zn(nba)2(meim)2 for adsorptive removal of eosin yellow dye from aqueous solution, Zeitschrift Fur Anorg. Und Allg. Chemie. 647 (2021) 1–12.

https://doi.org/10.1002/zaac.202000425.

[38] M.D. Olawale, A.C. Tella, J.A. Obaleye, J.S. Olatunji, Synthesis, characterization and crystal structure of a copper-glutamate metal organic framework (MOF) and its adsorptive removal of ciprofloxacin drug from aqueous solution, New J. Chem. 44 (2020) 3961–3969. https://doi.org/10.1039/d0nj00515k.

[39] A.C. Tella, A.C. Oladipo, V.O. Adimula, O.A. Ameen, S.A. Bourne, A.S. Ogunlaja, Synthesis and crystal structures of a copper(ii) dinuclear complex and zinc(ii) coordination polymers as materials for efficient oxidative desulfurization of dibenzothiophene, New J. Chem. 43 (2019) 14343–14354. https://doi.org/10.1039/c9nj01456j.

[40] O. V. Dolomanov, L.J. Bourhis, R.J. Gildea, J.A.K. Howard, H. Puschmann, OLEX2: A complete structure solution, refinement and analysis program, J. Appl. Crystallogr. 42 (2009) 339–341. https://doi.org/10.1107/S0021889808042726.

[41] G.M. Sheldrick, SHELXT - Integrated space-group and crystal-structure determination, Acta Crystallogr. Sect. A Struct. Chem. A71 (2015) 3–8.

[42] G.M. Sheldrick, Crystal structure refinement with SHELXL, Acta Crystallogr. Sect. C Struct. Chem. 71 (2015) 3–8. https://doi.org/10.1107/S2053229614024218.

[43] I. Ahmed, M. Tong, J.W. Jun, C. Zhong, S.H. Jhung, Adsorption of Nitrogen-Containing Compounds from Model Fuel over Sulfonated Metal-Organic Framework: Contribution of Hydrogen-Bonding and Acid-Base Interactions in Adsorption, J. Phys. Chem. C. 120 (2016) 407–415. https://doi.org/10.1021/acs.jpcc.5b10578.

[44] Z. Chen, L. Ling, B. Wang, H. Fan, J. Shangguan, J. Mi, Adsorptive desulfurization with metal-organic frameworks: A density functional theory investigation, Appl. Surf. Sci. 387 (2016) 483–490. https://doi.org/10.1016/j.apsusc.2016.06.078.

[45] E. Taşdemir, F.E. Özbek, M. Sertçelik, T. Hökelek, R.Ç. Çelik, H. Necefoğlu, Supramolecular complexes of Co(II), Ni(II) and Zn(II) p-hydroxybenzoates with caffeine: Synthesis, spectral characterization and crystal structure, J. Mol. Struct. 1119 (2016) 472–478. https://doi.org/10.1016/j.molstruc.2016.05.006.

[46] A. Alhadhrami, A.S.A. Almalki, A.M.A. Adam, M.S. Refat, Preparation of semiconductor zinc oxide nanoparticles as a photocatalyst to get rid of organic dyes existing factories in exchange for reuse in suitable purpose, Int. J. Electrochem. Sci. 13 (2018) 6503–6521. https://doi.org/10.20964/2018.07.04.

[47] H.F. McMurdie, E.H. Evans, M.C. Morris, B. Paretzkin, W. Wong-Ng, L. Ettlineer, C.R. Hubbard, Standard X-Ray Diffraction Powder Patterns from The JCPDS

Research Associateship, Powder Diffr. 1 (1986) 64–77. https://doi.org/10.1017/S0885715600011593.

[48] A.W. Addison, T.N. Rao, J. Reedijk, J. Van Rijn, G.C. Verschoor, Synthesis, structure, and spectroscopic properties of copper(II) compounds containing nitrogen-sulphur donor ligands; the crystal and molecular structure of aqua[1,7-bis(N-methylbenzimidazol-2′;-yl)-2,6-dithiaheptane]copper(II) perchlorate, J. Chem. Soc. Dalt. Trans. 7 (1984) 1349–1356. https://doi.org/10.1039/DT9840001349.

[49] M.A. Wani, A. Kumar, M.D. Pandey, R. Pandey, Heteroleptic 1D coordination polymers: 5-Coordinated zinc(II) polymer as an efficient transesterification catalyst, Polyhedron. 126 (2017) 142–149. https://doi.org/10.1016/j.poly.2017.01.027.

[50] A.M. Cheplakova, K.A. Kovalenko, D.G. Samsonenko, V.A. Lazarenko, V.N. Khrustalev, A.S. Vinogradov, V.M. Karpov, V.E. Platonov, V.P. Fedin, Metal-organic frameworks based on octafluorobiphenyl-4,4′-dicarboxylate: Synthesis, crystal structure, and surface functionality, Dalt. Trans. 47 (2018) 3283–3297. https://doi.org/10.1039/c7dt04566b.

[51] L.Y. Xin, Y.P. Li, F.Y. Ju, X.L. Li, G.Z. Liu, A supramolecular microporous network of zinc(II) coordination polymer for highly selective fluorescent detection of Pb2+, Indian J. Chem. - Sect. A Inorganic, Phys. Theor. Anal. Chem. 56A (2017) 826–831.

[52] J. Li, X. Zhang, B. Yue, A. Wang, L. Kong, J. Zhou, H. Chu, Y. Zhao, Preparation, crystal structure and luminescence properties of lanthanide complexes with 2,4,6-tri(Pyridin-2-yl)-1,3,5-triazine and organic carboxylic acid, Crystals. 7 (2017) 1–15. https://doi.org/10.3390/cryst7050139.

[53] F.A. Almeida Paz, J. Klinowski, Two- and three-dimensional cadmium-organic frameworks with trimesic acid and 4,4′-trimethylenedipyridine, Inorg. Chem. 43 (2004) 3882–3893. https://doi.org/10.1021/ic049523o.

[54] R. Subha, C. Namasivayam, Modeling of adsorption isotherm and kinetics of 2,4,6-Trichlorophenol onto microporous ZnCl2 activated coir pith carbon, J. Environ. Eng. Manag. 18 (2008) 275–280. https://pdfs.semanticscholar.org/e399/1d7171d901d5b17c601f83abe44dfe6d8386.pdf.

[55] Z.U. Zango, Z.N. Garba, N.H.H. Abu Bakar, W.L. Tan, M. Abu Bakar, Adsorption studies of Cu2 +–Hal nanocomposites for the removal of 2,4,6-trichlorophenol, Appl. Clay Sci. 132–133 (2016) 68–78. https://doi.org/10.1016/j.clay.2016.05.016.

[56] J. Fan, J. Zhang, C. Zhang, L. Ren, Q. Shi, Adsorption of 2,4,6-trichlorophenol from aqueous solution onto activated carbon derived from loosestrife, Desalination. 267

(2011) 139–146. https://doi.org/10.1016/j.desal.2010.09.016.

[57] R.M. Nthumbi, A.A. Adelodun, J.C. Ngila, Electrospun and functionalized PVDF/PAN composite for the removal of trace metals in contaminated water, Phys. Chem. Earth. 100 (2017) 225–235. https://doi.org/10.1016/j.pce.2016.08.007.

[58] P. Sejie, S. Nadiye-Tabbiruka, Removal of Methyl Orange (MO) from Water by adsorption onto Modified Local Clay (Kaolinite), Phys. Chem. 6 (2016) 39–48. https://doi.org/10.5923/j.pc.20160602.02.

[59] Z. Luo, M. Gao, Y. Ye, S. Yang, Modification of reduced-charge montmorillonites by a series of Gemini surfactants: Characterization and application in methyl orange removal, Appl. Surf. Sci. 324 (2015) 807–816. https://doi.org/10.1016/j.apsusc.2014.11.043.

[60] B.H. Hameed, Equilibrium and kinetics studies of 2,4,6-trichlorophenol adsorption onto activated clay, Colloids Surfaces A Physicochem. Eng. Asp. 307 (2007) 45–52. https://doi.org/10.1016/j.colsurfa.2007.05.002.

[61] M.H. Kalavathy, T. Karthikeyan, S. Rajgopal, L.R. Miranda, Kinetic and isotherm studies of Cu(II) adsorption onto H3PO 4-activated rubber wood sawdust, J. Colloid Interface Sci. 292 (2005) 354–362. https://doi.org/10.1016/j.jcis.2005.05.087.

[62] L. Cui, X. Guo, Q. Wei, Y. Wang, L. Gao, L. Yan, T. Yan, B. Du, Removal of mercury and methylene blue from aqueous solution by xanthate functionalized magnetic graphene oxide: Sorption kinetic and uptake mechanism, J. Colloid Interface Sci. 439 (2015) 112–120. https://doi.org/10.1016/j.jcis.2014.10.019.

[63] S. Nethaji, A. Sivasamy, A.B. Mandal, Preparation and characterization of corn cob activated carbon coated with nano-sized magnetite particles for the removal of Cr(VI), Bioresour. Technol. 134 (2013) 94–100. https://doi.org/10.1016/j.biortech.2013.02.012.

[64] M. Raoov, S. Mohamad, M.R. Abas, Removal of 2,4-dichlorophenol using cyclodextrin-ionic liquid polymer as a macroporous material: Characterization, adsorption isotherm, kinetic study, thermodynamics, J. Hazard. Mater. 263 (2013) 501–516. https://doi.org/10.1016/j.jhazmat.2013.10.003.

[65] M. Karamipour, S. Fathi, M. Safari, Removal of phenol from aqueous solution using MOF / GO : Synthesis , characteristic , adsorption performance and mechanism, Int. J. Environ. Anal. Chem. 00 (2021) 1–12. https://doi.org/10.1080/03067319.2021.1915299.

[66] N. Yadav, D.N. Maddheshiaya, S. Rawat, J. Singh, Adsorption and equilibrium studies

of phenol and para-nitrophenolby magnetic activated carbon synthesised from cauliflower waste, Environ. Eng. Res. 25 (2020) 742–752.

[67] Z. Wu, X. Yuan, H. Zhong, H. Wang, G. Zeng, X. Chen, H. Wang, L. Zhang, J. Shao, Enhanced adsorptive removal of p-nitrophenol from water by aluminum metal-organic framework/reduced graphene oxide composite, Sci. Rep. 6 (2016) 1–13. https://doi.org/10.1038/srep25638.

[68] M. Radhika, K. Palanivelu, Adsorptive removal of chlorophenols from aqueous solution by low cost adsorbent-Kinetics and isotherm analysis, J. Hazard. Mater. 138 (2006) 116–124. https://doi.org/10.1016/j.jhazmat.2006.05.045.

[69] I.A.W. Tan, A.L. Ahmad, B.H. Hameed, Preparation of activated carbon from coconut husk: Optimization study on removal of 2,4,6-trichlorophenol using response surface methodology, J. Hazard. Mater. 153 (2008) 709–717. https://doi.org/10.1016/j.jhazmat.2007.09.014.

[70] I.A.W. Tan, A.L. Ahmad, B.H. Hameed, Adsorption isotherms, kinetics, thermodynamics and desorption studies of 2,4,6-trichlorophenol on oil palm empty fruit bunch-based activated carbon, J. Hazard. Mater. 164 (2009) 473–482. https://doi.org/10.1016/j.jhazmat.2008.08.025.

[71] B.H. Hameed, I.A.W. Tan, A.L. Ahmad, Preparation of oil palm empty fruit bunch-based activated carbon for removal of 2,4,6-trichlorophenol: Optimization using response surface methodology, J. Hazard. Mater. 164 (2009) 1316–1324. https://doi.org/10.1016/j.jhazmat.2008.09.042.

[72] A.M. Oliveira, M.A.L. Milhome, T. V. Carvalho, R.M. Cavalcante, R.F. Nascimento, Use of Low-cost Adsorbents to Chlorophenols and Organic Matter Removal of Petrochemical Wastewater, Orbital - Electron. J. Chem. 5 (2013) 171–178. https://doi.org/10.17807/orbital.v5i3.477.

[73] M.O. Aremu, A.O. Alade, A.A. Bello, K.K. Salam, Kinetics and Thermodynamics of 2,4,6–Trichlorophenol Adsorption onto Activated Carbon Derived from Flamboyant Pod Bark, J. Int. Environ. Appl. Sci. 13 (2018) 158–166.